Materials Horizons

ROYAL SOCIETY OF CHEMISTRY

COMMUNICATION

View Article Online
View Journal

Cite this: DOI: 10.1039/d5mh01737h

Received 12th September 2025,
Accepted 2nd April 2026

DOI: 10.1039/d5mh01737h

rsc.li/materials-horizons

Emergence of magnetic monopole-like behavior in iron oxide nanoparticles grafted with chiral brushes: a chiral induced spin selectivity manifestation

Elizabeth Shiby, †[a] Yu Shao,†[bc] Minh Dang Nguyen, †[d] Puja Thapa,[e] Supriya Ghosh,[a] Ishwari Chaitanya Joshi,[b] Yuming Huang,[b] Supawitch Hoijang,[d] Ramtin Yarinia,[d] Christopher K. Ober,[b] T. Randall Lee,[d] Dali Sun,[e] Brian P. Bloom *[a] and David H. Waldeck ‡[a]

We examine the magnetic properties of ~23 nm single domain nanocubes and ~200 nm multidomain iron oxide nanoparticles that are surface functionalized with poly(L- or D-phenylalanine) chiral brushes of variable length. Interestingly, the larger nanoparticles manifest a remanent magnetization in all directions, *i.e.*, display monopole-like or hedgehog behaviour that depends on the handedness of the brush. Conversely, no such response is observed in the smaller nanoparticles. The emergent monopole-like magnetic properties are attributed to the chiral-induced spin selectivity effect acting on the magnetic domain structure, single *vs.* multidomain, to imprint a magnetization bias on the nanoparticles. Collectively, this study reveals a facile approach for the formation of hedgehog magnetic nanoparticles and outlines features necessary for their formation.

New concepts

This work presents a new design strategy for creating hedgehog (anti-hedgehog) nanoparticles through the chiral-induced spin selectivity effect (CISS). Here, we rely on the organization of magnetic dipoles, generated through interactions between multidomain iron oxide nanoparticles and surface grafted chiral polymers, to create monopole-like behaviour. Our magnetic force microscopy measurements show a robust inward or outward magnetization that depends on the enantiomeric form of the grafted polymer. In contrast, no hedgehog behaviour is observed in the single domain nanoparticles with smaller size, and the difference is attributed to antisymmetric coupled spin alignment within a single domain assisted by Dzyaloshinskii–Moriya interaction (DMI). These results are corroborated by magnetometry measurements which indicate the coexisting of a CISS-tailored hedgehog magnetic configuration and regular non-CISS magnetic domains within the multidomain structure of large-sized nanoparticles. This innovative strategy demonstrates a facile approach for creating monopole-like behaviour that may prove useful for next-generation data storage, nanomedicine, and energy conversion technologies.

1. Introduction

The concept of a magnetic dipole originates from a multipole expansion of the vector potential for a distribution of current in a system.[1] Maxwell's equations predict that the reduction of a magnetic dipole to a magnetic monopole cannot occur, because the total vector displacement in a closed loop is always zero.[1] In 1931 however, Dirac showed that quantum mechanics allows for the existence of magnetic monopoles without violating Maxwell's equations.[2] While the existence of fundamental magnetic monopoles remains a point of contention,[3–5] its attractiveness for revolutionizing the fields of spintronics, data storage, *etc.* has led to continuous research both in particle physics and into the creation of metamaterials, which behave like a monopole.[6,7] For instance, experimental evidence for monopole-like behaviour has been observed in spin ices, including lanthanide pyrochlore magnetic insulators like $Dy_2Ti_2O_7$, and with skyrmions; however, these phenomena are observed at low temperatures and/or under specialized conditions.[8–11] In an alternative approach, researchers have shown that the spatial arrangement of magnetic dipoles at a material's surface can give rise to emergent monopole-like behaviour. Referred to as hedgehog (anti-hedgehog) magnetic particles, or Bloch points,[12,13] the topology of magnetic dipoles at the surface of a spherical object are structured in such a way that all the magnetic dipole moments are oriented outward (or inward) along the normal of the object's surface.

[a] *Department of Chemistry, University of Pittsburgh, Pittsburgh, Pennsylvania, 15260, USA. E-mail: bpb8@pitt.edu*
[b] *Department of Materials Science and Engineering, Cornell University, Ithaca, New York, 14853, USA*
[c] *Chemical and Biomolecular Engineering, University of Notre Dame, South Bend, Indiana, 46637, USA*
[d] *Department of Chemistry and the Texas Center for Superconductivity, University of Houston, Houston, Texas, 77204, USA*
[e] *Department of Physics & Astronomy, North Carolina State University, Raleigh, North Carolina, 27695, USA*
† These authors contributed equally to this work.
‡ Deceased.

The chiral-induced spin selectivity (CISS) effect conventionally refers to the generation of spin polarization by way of electron displacement currents in a chiral molecule or material[14,15] and has recently shown promise for altering magnetic properties of materials.[16,17] For instance, chiral molecules assembled onto Hall devices exhibit Hall and anomalous Hall effects upon charge polarization;[18–20] and chiral self-assembled monolayers (SAMs) adsorbed onto patterned, thin-film ferromagnetic substrates can give rise to a remanent magnetization of the substrate in the absence of an external magnetic field.[21] Additionally, the CISS effect can be used to change the magnetic properties of a material.[22] Although the manipulation and control of the electron spin through chirality, has been leveraged to create spin-LEDs, memristors/transistors, and magnetic memory devices,[23–29] it has not yet been used to create materials that behave as magnetic monopoles.

To date, CISS-based manifestations of remanent magnetization have focused on planar systems decorated with chiral molecules; however, we hypothesize that these findings can be extrapolated to zero-dimensional objects, namely nanoparticles, and manifest hedgehog (anti-hedgehog) behaviour under ambient conditions. Indeed, similar arguments have been made previously; Zhu *et al.* showed that the pulling force required to detach chiral superparamagnetic iron oxide nanoparticles (SPIONs) adsorbed on an atomic force microscopy (AFM) tip from a ferromagnetic substrate is influenced by the particle's handedness and direction of magnetization of the ferromagnetic substrate.[30] The asymmetric response was attributed to monopole-like behaviour. As the authors point out, however, they perform a contact-mode measurement, and the pulling force differences have important contributions from spin-exchange interactions, which could display a similar magnetic field-dependent response as one would find for a monopole. Previous reports indicate that the contact potential difference of chiral materials assembled on ferromagnetic surfaces can change with applied magnetic field, owing to differences in spin exchange interactions at the material-ferromagnetic interface.[31] Further evidence is provided in work by Ghosh *et al.* in which magnetic force microscopy (MFM) measurements, a non-contact method of measuring magnetic properties, on chiral molecule-coated SPIONs did not exhibit any field-dependent changes in magnetic properties.[22]

Herein, we synthesize iron oxide (Fe_3O_4) nanoparticles (NPs) of different sizes, coated with chiral brushes, and we perform MFM measurements that suggest the emergence of hedgehog NPs through the CISS effect. Distinguishable magnetic properties becomes manifest with particle domain size. For multidomain NPs, the sign of the remanent magnetization is shown to depend on the handedness of the chiral brush coating. These findings are corroborated by superconducting quantum interference device SQUID magnetometry measurements, and the effects are attributed to the emergence of CISS-induced hedgehog antisymmetric exchange coupling in the multidomain adjacent to the surface of large-sized NPs. We conclude with a forward-looking roadmap on how fine-control over the NP-chiral brush properties will further elucidate our understanding of the working mechanism in this interesting system and lead to next-generation chiral hedgehog materials through exploitation of the CISS effect.

2. Results and discussion

In this work, two sizes of Fe_3O_4 NPs grafted with chiral polymers—poly(L- or D-phenylalanine) (L- or D-Phe)—are studied: 23 nm single domain ferrimagnetic (FiM) Fe_3O_4 nanocubes and 203 nm multidomain superparamagnetic (SPM) Fe_3O_4 nanospheres. Note that, these sizes reflect the size before polymer grafting, and the magnetic properties were determined and reported previously.[32] In addition, we compare the new results from this study with a third size regime (10–20 nm), based on our previous work involving SPIONs passivated with L- or D-tartaric acid.[22] Details of the synthesis of SPIONs *via* a thermal decomposition method and their surface passivation with L- and D-tartaric acid *via* a ligand exchange method, including characterization, were reported in that previous study.[22] The two larger Fe_3O_4 NPs, featuring different magnetic domain structures, were synthesized following previously reported procedures.[32] Briefly, the 23 nm FiM Fe_3O_4 nanocubes were prepared *via* a thermal decomposition method, whereas the 203 nm SPM Fe_3O_4 nanospheres were produced using a solvothermal method. The resulting NPs were subsequently encapsulated within a silica shell (Fe_3O_4@SiO_2) and functionalized with amine groups prior to surface decoration with poly(L-Phe) and poly(D-Phe) *via* surface-initiated ring-opening polymerization of *N*-carboxy anhydride (NCA) monomers, as illustrated in Scheme 1. Details of the synthesis and characterization of these NPs and the multidomain SPM NPs, including their surface grafting with the chiral polymers, are provided in the Experimental section.

Fig. 1a-i and b-i show representative TEM images of the FiM single-domain and SPM multidomain Fe_3O_4 NPs, respectively, after silica coating and surface functionalization with 3-aminopropyltriethoxysilane (APTES). The size distribution of the pristine NPs (before silica coating and APTES functionalization) indicates an average edge length of 23 ± 3 nm for the FiM single-domain nanocubes and an average diameter of 203 ± 12 nm for the SPM multidomain nanospheres (see Fig. S1). In addition, the XRD patterns of the pristine Fe_3O_4 NPs correspond with the Fe_3O_4 (magnetite) phase, according to JCDPS No. 01-088-0315 (see Fig. S2). Following silica coating, the particle sizes for both types of Fe_3O_4 cores increase, see Fig. 1a-i and b-i; the average shell thicknesses for the 23 nm

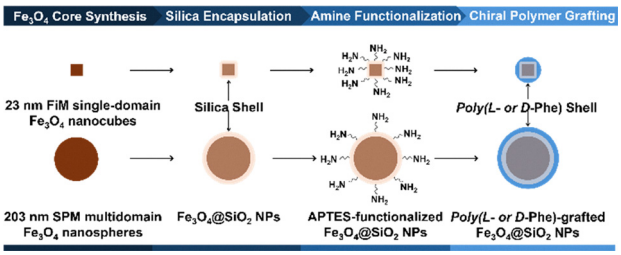

Scheme 1 Schematic illustration of the synthesis steps for poly(L- or D-Phe)-grafted Fe_3O_4 NPs.

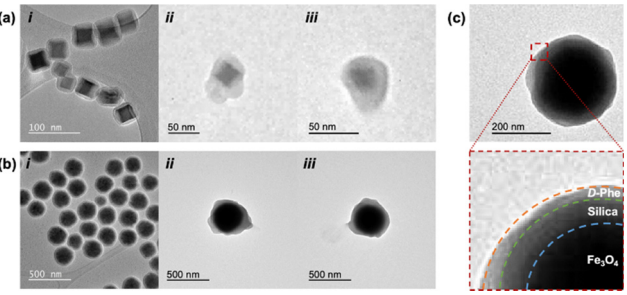

Fig. 1 TEM images of (a) 23 nm FiM single-domain and (b) 203 nm SPM multidomain Fe_3O_4 NPs: (i) after silica coating and amine functionalization (achiral NPs), and after subsequent grafting with (ii) poly(L-Phe) and (iii) poly(D-Phe). (c) Higher-magnification TEM images of poly(D-Phe)-grafted 203 nm SPM multidomain Fe_3O_4 NPs.

FiM single-domain and the 200 nm SPM multidomain Fe_3O_4 cores were 3 ± 1 nm and 20 ± 2 nm, respectively. The silica-coated Fe_3O_4 NPs were then functionalized with APTES prior to growth of the chiral polymer brushes. High-resolution N 1s XPS spectra reveal a peak at a binding energy of $\sim$399 eV, indicating the presence of amine groups from the APTES molecules (see Fig. S3).[33] Additionally, no significant change in shell thickness was observed for either type of magnetic core particles after APTES functionalization. These results confirm the successful synthesis of amine-functionalized Fe_3O_4@SiO_2 NPs for growing the chiral polymer brushes.

Next, the NPs were grafted with chiral brushes, poly(L- or D-Phe), *via* surface-initiated ring-opening polymerization of NCA.[34] TEM images show an additional layer surrounding the silica-coated NPs, indicating successful attachment of the chiral polymers (see Fig. 1a-ii, iii and b-ii,iii). In addition, higher-magnification TEM images of representative chiral polymer-grafted NPs—specifically, poly(D-Phe)-coated 203 nm SPM multidomain Fe_3O_4 NPs—clearly show the presence of a polymer shell in addition to the silica shell (see Fig. 1c). Further characterization of the NPs grafted with the chiral brushes is provided in the Supporting Information (see Fig. S4–S7). Note that the fast ring-opening kinetics of the NCA and poor solubility of the polymers result in polymer coatings of variable thickness; however, the size of the NP core, *i.e.*, the Fe_3O_4@SiO_2, remains unchanged.

To investigate the magnetic properties of the NPs with chiral brushes, MFM was performed using previously established protocols.[22,35,36] The technique is a type of AFM that uses a magnetized tip to detect magnetic interactions between the tip and the material—in this case, a NP. This process is schematically summarized in Fig. S8a. To perform MFM, a conductive CoCr tip was magnetized with a 0.5 T permanent magnet prior to measurements. Scans were first performed with the tip magnetized in one direction (South), followed by re-measurement of the same NP with the opposite magnetization (North). It is noted that all of the measurements were performed at a constant lift height of 125 nm in order to minimize electrostatic interactions, and the phase shift was referenced to the background of a bare Au substrate. Fig. 2a–d shows representative AFM topography images along with corresponding height profiles of 23 nm FiM single-domain and 203 nm SPM multidomain Fe_3O_4 NPs grafted

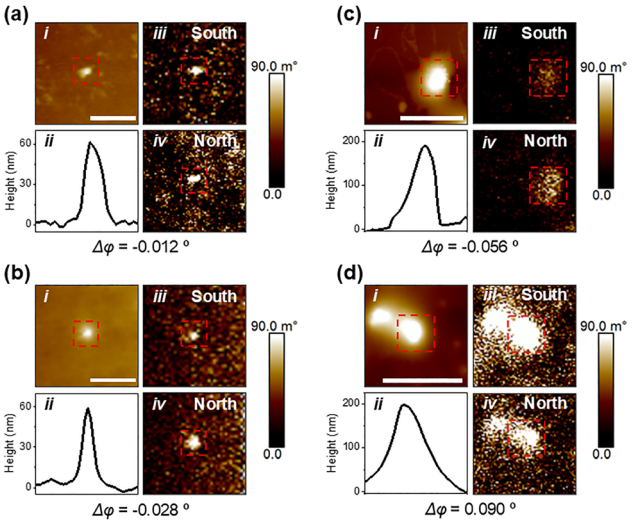

Fig. 2 Panels (a–d) shows AFM topography (i), height profiles (ii) of a given NP, and corresponding MFM images with a South (iii) and North (iv) magnetized tip for each panel. Panel (a) shows L- and panel (b) shows D-Phe-coated 23 nm FiM single-domain Fe_3O_4 nanocubes and panel (c) shows L- and panel (d) shows D-Phe-coated 203 nm SPM multidomain Fe_3O_4 nanospheres. The red square indicates the measured nanoparticle and the change in phase, $\Delta\varphi$, is reported beneath each panel in degrees, °. The scale bar corresponds to 2 μm.

with L- and D-Phe chiral brushes. Each panel also includes corresponding MFM images of the same particle, acquired using both South- and North-magnetized tips. Darker regions indicate lower phase shifts corresponding to attractive magnetic interactions, whereas brighter regions represent higher phase shifts associated with repulsive interactions. In addition, the difference in phase shift with field direction ($\Delta\varphi = \varphi_S - \varphi_N$, where φ_S and φ_N correspond to the phase shift obtained with South- and North-magnetized tips, respectively) is shown in each panel. The 23 nm L- and D-Phe FiM single-domain Fe_3O_4 NPs show no significant difference in phase shift with tip magnetization, and the sign of the phase shift is independent of the brush chirality. Conversely, the 203 nm SPM multidomain Fe_3O_4 NPs exhibit an enantiospecific response, L-chiral brush coatings show an increased phase shift (indicative of repulsive interactions) with a North-magnetized tip, whereas D-chiral brush coatings reveal an increased phase shift with a South-magnetized tip. Note that, additional measurements on a different set of NPs are shown in Fig. S8b–e.

Because MFM imaging is prone to artifacts, we further evaluated the magnetic response of >30 individual L- and D-chiral brush-coated single domain and multi-domain Fe_3O_4 NPs. Note that, for each individual NP the same AFM tip is used to measure both magnetizations. To account for the variation in magnitude of the phase shift from particle to particle, as well as tip-NP distances associated with polymer brushes of varying length, we compare the magnetic properties for the different systems by defining a phase shift asymmetry parameter, g_φ, as

$$g_\varphi = \frac{\varphi_S - \varphi_N}{\varphi_S + \varphi_N}$$

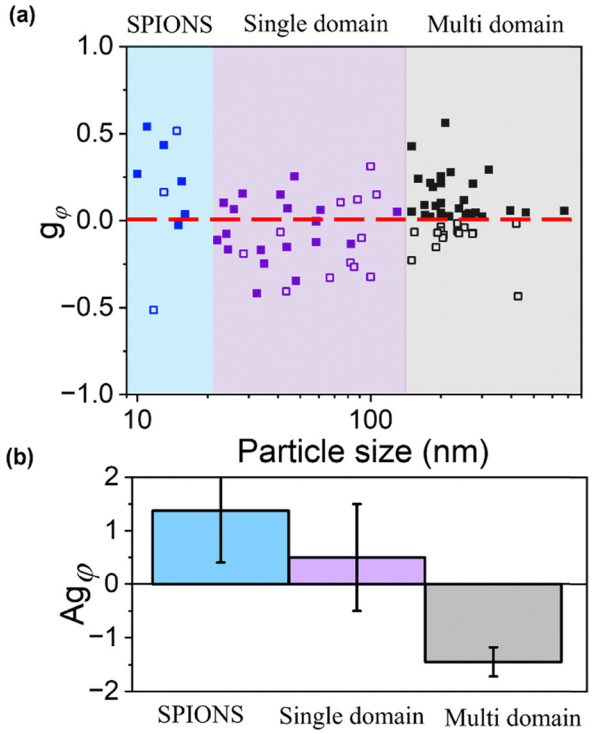

Fig. 3 Panel (a) shows the correlation between the asymmetry in phase shift, g_φ, of SPIONs (blue), 23 nm FiM single-domain (purple), and 203 nm SPM multidomain (black) Fe_3O_4 NPs as a function of size. The filled and open symbols represent the D- and L-isomer of the chiral ligand or brush, respectively. The g_φ data on SPIONs is replotted from Ref. 22, with permission. The red dashed line is a visual guide to the eye, set to $g_\varphi = 0$. Panel (b) plots a corresponding anisotropy measure, Ag_φ for each particle type. The same color coding is used in panel (a) and the error bars represent the propagated errors for the standard deviation of the mean.

where φ_S and φ_N are the phase shifts recorded under a South and a North magnetized tip, respectively.

Fig. 3a compares g_φ for L- and D-chiral brush-coated FiM single-domain Fe_3O_4 NPs (purple) and SPM multidomain Fe_3O_4 NPs (gray) as a function of the particle size after functionalization with the chiral brush. In addition, data on L- and D-tartaric acid-passivated SPIONs, replotted from our previous study,[22] is also included (blue). Note that the spread in particle size for the FiM and SPM NPs is associated with particle-to-particle variation in polymer growth. The L- ligands and brushes are denoted with an open symbol and the D- ligands and brushes with a closed symbol. Both the SPIONs and FiM single-domain Fe_3O_4 NPs show no dependence on the handedness of the chiral molecule used for surface passivation and the magnetic response measured by MFM; *i.e.*, both positive and negative g_φ are observed for each isomer. In contrast, the L- and D-chiral brush-coated SPM multidomain Fe_3O_4 NPs exhibit a robust chirality-dependent magnetic response; g_φ values are consistently positive for Fe_3O_4 NPs with D-chiral brushes and negative for those with L-chiral brushes. Note that, the magnitude of g_φ is independent of particle size and implies that the asymmetry in local magnetic environment is unaffected by polymer length.

Fig. 3b plots an anisotropy measure, Ag_φ for the two enantiomers, *i.e.* $Ag_\varphi = \frac{\overline{g_{\varphi D}}}{\overline{g_{\varphi L}}}$ where $\overline{g_{\varphi D}}$ and $\overline{g_{\varphi L}}$ represents the average g_φ of D and L isomer respectively. A positive Ag_φ indicates that the sign of average phase shift is independent of the enantiomeric form of the chiral ligand/brush, whereas a negative Ag_φ implies that magnetic response is opposite for the two enantiomorphs. For SPIONs and FiM single-domain Fe_3O_4 NPs Ag_φ is greater than 0, *i.e.* the magnetic properties are not correlated with the handedness of the ligands/brushes, whereas for SPM multidomain NPs Ag_φ is negative, *i.e.* the sign of the magnetization strongly correlates with the chirality of the brush. To validate the role of the chiral brush for determining the magnetic response, additional MFM measurements were performed on 203 nm SPM multidomain Fe_3O_4 NPs without a chiral brush, and no consistent phase shift was observed (see Fig. S9). We attribute the enantiospecific response associated with brush chirality to the formation of hedgehog (anti-hedgehog) magnetic structure on the NP. Interestingly, no dependence on brush length with g_φ value was observed and implies that CISS acting on the NPs is likely operating in a saturated regime.

We propose a qualitative model to explain the emergence of hedgehog NP behaviour in SPM Fe_3O_4 NPs in contrast to the FiM single-domain Fe_3O_4 NPs. For traditional NPs with small size, the presence of magnetism could be described by the superparamagnetic model of which the blocking temperature is determined by the magnetic anisotropy and volume of the NPs. The small NPs' blocking temperature would be usually lower than accessible temperatures due to the thermal fluctuations. We propose that this situation is changed when the chiral molecules are incorporated. Here we posit that the chiral molecule brushes in the NPs induce a radial, antisymmetric exchange coupling term on the magnetic ordering of the NPs, *i.e.*, Dzyaloshinskii-Moriya interaction (DMI).[37] In the case of SPIONs and FiM single-domain Fe_3O_4 NPs, this extra antisymmetric exchange coupling stemming from the chiral molecules modified the NPs' magnetic properties; see Fig. 4a. Instead of increasing the magnetic anisotropic or volume of NPs, this DMI term leads to an extra exchange coupling that stabilizes the magnetic moments against the thermal fluctuations, similar to skyrmions (Fig. 4c) which is wholly different from that observed in NPs without chiral brushes (Ref. 38). The radial magnetic configuration from the chiral molecules (small light red arrows) within a single domain does not lead to a net outward or inward moment because all of the spins must be aligned. Thereby the CISS-induced DMI cannot create an outwardly or inwardly oriented remanent magnetization because it clashes with the material's magnetic domain so that a g_φ which is consistent with the chiral molecules' handedness is not observed. Conversely, for multidomain particles with much larger size, when chiral brushes are grafted onto the surface, these domains interact locally with chiral molecules where the DMI persists, leading to a net outward or inward magnetization that depends on the handedness of the chiral brushes due to curvature of the surface. Thus, a hedgehog (anti-hedgehog) NP (see Fig. 4b) is created. Note that, the chirality transfer and its DMI merely affects the small-sized domain adjacent to the surface as the size of the single domain. There

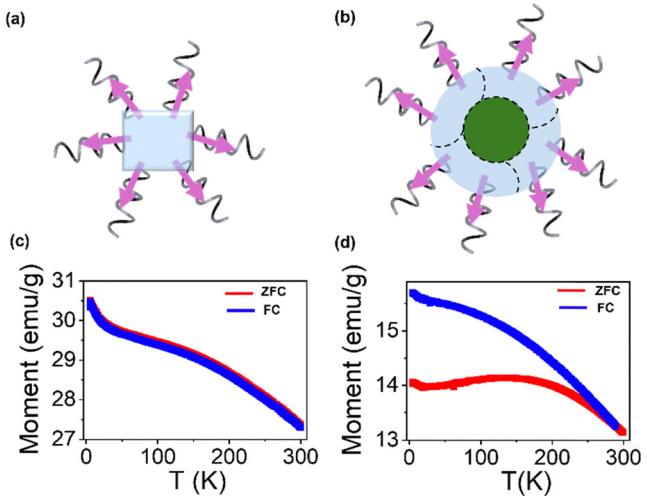

Fig. 4 Panels (a) and (b) show schematic representations of a single-domain NP and multidomain NP coated with chiral polymer brushes (gray helices). The outward magnetic field driven by the CISS effect (light red arrow) acts uniformly on the NPs. Because spins within a domain must all align along the same direction, the magnetization state of a single-domain NP becomes frustrated and cannot accommodate the uniform field induced by the ligands. Conversely, for a multidomain NP, each domain (black dashed line) can possess its own magnetization state and locally align with the magnetic field induced by the chiral ligands. This phenomenon results in a net outward magnetic moment of the NP, *i.e.*, monopole-like behaviour. Panels (c) and (d) show the *M*–*T* curves under field cooling (FC) and zero-field cooling (ZFC) conditions for the single-domain and multidomain Fe_3O_4 NPs modified with D-chiral brushs, respectively.

would be magnetic domains in the center that are prone to the CISS effect of which their blocking temperature remains low. This induces the reduced blocking temperature for the large-sized NPs as seen from temperature dependence of magnetization (*M*–*T*) curvein Fig. 4d compared to what is observed in Fig. 4c for smaller NPs. As described by the theoretical model in the earlier manuscript by Zhu,[30] this behaviour results because the magnetic moments between domains within the particle largely cancel each other while those on the surface are pointed uniformly outward.

3. Conclusions

This work highlights the potential of the CISS effect to modulate the magnetic behaviour of materials towards the creation of hedgehog NPs. Through an in-depth series of MFM experiments, we observed a distinct chirality-dependent magnetic interaction in multidomain Fe_3O_4 NPs functionalized with chiral brushes that is reminiscent of magnetic monopole behaviour. Conversely, analogous single-domain NPs and systems without chiral brushes did not lead to a consistent dependence of the magnetic response. While our studies show that the anisotropy in phase shift with magnetic field does not depend on polymer length, at least under the conditions studied in this work, it is unclear how the size of the Fe_3O_4 NPs and the SiO_2 shell thickness impact the hedgehog (anti-hedgehog) behaviour. Future studies must consider these design features for further leveraging the ordering temperature of small NPs using different chiral ligands in which the CISS response can be tailored. Additionally, domain mapping of the magnetic structure like Lorentz Transmission Electron Microscopy and rigorous theoretical modelling is necessary to confirm the proposed DMI model. Regardless, this work provides compelling evidence for chirality-driven magnetic modulation of materials, underscoring the potential of chiral surface functionalization as a powerful tool for designing spin selective nanomaterials for applications in spintronics.

Conflicts of interest

There are no conflicts to declare.

Data availability

The data supporting the findings of this study are available from the corresponding author on reasonable request.

Supplementary information (SI): Experimental section; size distribution of 23 nm FiM single-domain and 203 nm SPM multidomain Fe_3O_4 NPs (Fig. S1); XRD patterns of 23 nm FiM single-domain and 203 nm SPM multidomain Fe_3O_4 NPs, including JCPDS No. 01-088-0315 (Fig. S2); high-resolution N 1s XPS spectra of APTES-functionalized Fe_3O_4 NPs composed of 23 nm FiM single-domain and 203 nm SPM multidomain Fe_3O_4 cores (Fig. S3); ^{1}H NMR of L- and D-Phe NCA monomers (Fig. S4); ^{13}C NMR of L- and D-Phe NCA monomers (Fig. S5); CD spectra of the polymers grafted on NPs (Fig. S6) FTIR and TGA of NPs (Fig. S7); Schematic of MFM measurement and additional MFM images of the NPs (Fig. S8) the correlation between asymmetry in phase shift, g_φ, with the radius of achiral 203 nm SPM multidomain Fe_3O_4 NPs (Fig. S9). M–H curves of single-domain and multidomain Fe_3O_4 NPs (Fig. S10). See DOI: https://doi.org/10.1039/d5mh01737h.

Acknowledgements

T. R. Lee thanks the Air Force Office of Scientific Research (FA9550-23-1-0581; 23RT0567) and the Robert A. Welch Foundation (Grant No. E-1320 and V-E-0001) for their financial support of the research at the University of Houston. C. K. Ober would like to extend their gratitude to the Air Force Office of Scientific Research (AFOSR FA9550-22-1-0524) and Cornell Center for Materials Research Shared Facilities, which is supported through the NSF MRSEC program (DMR-1719875). D. Sun acknowledges financial support from the Air Force Office of Scientific Research, MURI Program under award number FA9550-23-1-0311. D. H. Waldeck acknowledges financial support from the Air Force Office of Scientific Research, MURI Program under award number FA9550-23-1-0368.

Notes and references

1 D. J. Griffiths, *Introduction to Electrodynamics*, Cambridge University Press, 2023.

2 P. A. M. Dirac, Quantized Singularities in the Electromagnetic Field, *Proc. R. Soc. London, Ser. A*, 1931, **133**, 60–72.
3 K. A. Milton, Theoretical and Experimental Status of Magnetic Monopoles, *Rep. Prog. Phys.*, 2006, **69**, 1637–1711.
4 A. Rajantie, The Search for Magnetic Monopoles, *Phys. Today*, 2016, **69**, 40–46.
5 A. Rajantie, Introduction to Magnetic Monopoles, *Contemp. Phys.*, 2012, **53**, 195–211.
6 P. Benes, F. Blaschke and Y. M. Cho, Electroweak Monopole-Antimonopole Pair Production at LHC, Ver. 4., *arXiv*, 2024, preprint, arXiv:2403.10747, DOI: 10.48550/arXiv.2403.10747.
7 B. Acharya, J. Alexandre, P. Benes, B. Bergmann, S. Bertolucci, A. Bevan, H. Branzas, P. Burian, M. Campbell, Y. M. Cho, M. de Montigny, O. Gould, J. Hays, A. M. Hirt, D. L.-J. Ho, P. Q. Hung, J. Janecek, M. Kalliokoski, A. Korzenev, D. H. Lacarrère, C. Leroy, G. Levi, A. Lionti, A. Maulik, A. Margiotta, N. Mauri, N. E. Mavromatos, P. Mermod, L. Millward, V. A. Mitsou, I. Ostrovskiy, P.-P. Ouimet, J. Papavassiliou, B. Parker, L. Patrizii, G. E. Păvălaș, J. L. Pinfold, L. A. Popa, V. Popa, M. Pozzato, S. Pospisil, A. Rajantie, R. R. de Austri, Z. Sahnoun, M. Sakellariadou, A. Santra, S. Sarkar, G. Semenoff, A. Shaa, G. Sirri, K. Sliwa, R. Soluk, M. Spurio, M. Staelens, M. Suk, M. Tenti, V. Togo, J. A. Tuszyn'ski, A. Upreti, V. Vento and O. Vives, Search for Magnetic Monopoles Produced via the Schwinger Mechanism, *Nature*, 2022, **602**, 63–67.
8 Q. N. Meier, M. Fechner, T. Nozaki, M. Sahashi, Z. Salman, T. Prokscha, A. Suter, P. Schoenherr, M. Lilenblum, P. Borisov, I. E. Dsyaloshinkskii, M. Fiebig, H. Luetkens and N. A. Spaldin, Search for the Magnetic Monopole at a Magnetoelectric Surface, *Phys. Rev. X*, 2019, **9**, 011011.
9 C. Castelnovo, R. Moessner and S. L. Sondhi, Magnetic Monopoles in Spin Ice, *Nature*, 2008, **451**, 42–45.
10 R. Dusad, F. K. K. Kirschner, J. C. Hoke, B. R. Roberts, A. Eyal, F. Flicker, G. M. Luke, S. J. Blundell and J. C. S. Davis, Magnetic Monopole Noise, *Nature*, 2019, **571**, 234–239.
11 N. A. Spaldin, M. Fechner, E. Bousquet, A. Balatsky and L. Nodrstrom, Monopole-based Formalism for the Diagonal Magnetoelectric Response, *Phys. Rev. B:Condens. Matter Mater. Phys.*, 2013, **88**, 094429.
12 A. Rana, C.-T. Liao, E. Iacocca, J. Zou, M. Pham, X. Lu, E.-E. C. Subramanian, Y. H. Lo, S. A. Ryan, C. S. Bevis, R. M. Karl, A. J. Glaid, J. Rable, P. Mahale, J. Hirst, T. Ostler, W. Liu, C. M. O'Leary, Y.-S. Yu, K. Bustillo, H. Ohldag, D. A. Shapiro, S. Yazdi, T. E. Mallouk, S. J. Osher, H. C. Kapteyn, V. H. Crespi, J. V. Badding, Y. Tserkovnyak, M. M. Murnane and J. Miao, Three-Dimensional Topological Magnetic Monopoles and Their Interactions in a Ferromagnetic Meta-Lattice, *Nat. Nanotechnol.*, 2023, **18**, 227–232.
13 X.-L. Qi, R. Li, J. Zang and S.-C. Shang, Inducing a Magnetic Monopole with Topological Surface States, *Science*, 2009, **323**, 1184–1187.
14 R. Naaman, Y. Paltiel and D. H. Waldeck, Chiral molecules and the electron spin, *Nat. Rev. Chem.*, 2019, **3**, 250–260.
15 B. P. Bloom, Y. Paltiel, R. Naaman and D. H. Waldeck, Chiral Induced Spin Selectivity, *Chem. Rev.*, 2024, **124**, 1950–1991.
16 O. Ben Dor, N. Morali, S. Yochelis, L. T. Baczewski and Y. Paltiel, Local Light-Induced Magnetization Using Nanodots and Chiral Molecules, *Nano Lett.*, 2014, **14**, 6042–6049.
17 I. Carmeli, G. Leitus, R. Naaman, S. Reich and Z. Vager, Magnetism Induced by the Organization of Self-Assembled Monolayers, *J. Chem. Phys.*, 2003, **118**, 10372–10375.
18 M. Eckshtain-Levi, E. Capua, S. Refaely-Abramson, S. Sarkar, Y. Gavrilov, S. P. Mathew, Y. Paltiel, Y. Levy, L. Kronik and R. Naaman, Cold Denaturation Induces Inversion of Dipole and Spin Transfer in Chiral Peptide Monolayers, *Nat. Commun.*, 2016, **7**, 10744.
19 E. Z. Smolinsky, A. Neubauer, A. Kumar, S. Yochelis, E. Capua, R. Carmieli, Y. Paltiel, R. Naaman and K. Michaeli, Electric Field Controlled Magnetization in GaAs/AlGaAs Heterostructures–Chiral Organic Molecules Hybrids, *J. Phys. Chem. Lett.*, 2019, **10**, 1139–1145.
20 A. Kumar, E. Capua, M. K. Kesharwani, J. M. L. Martin, E. Sitbon, D. H. Waldeck and R. Naaman, Chirality-Induced Spin Polarization Places Symmetry Constraints on Biomolecular Interactions, *Proc. Natl. Acad. Sci. U. S. A.*, 2017, **114**, 2474–2478.
21 O. Ben Dor, S. Yochelis, A. Radko, K. Vankayala, E. Capua, A. Capua, S. H. Yang, L. T. Baczewski, S. S. P. Parkin, R. Naaman and Y. Paltiel, Magnetization Switching in Ferromagnets by Adsorbed Chiral Molecules without Current or External Magnetic Field, *Nat. Commun.*, 2017, **8**, 14567.
22 G. Koplovitz, G. Leitus, S. Ghosh, B. P. Bloom, S. Yochelis, D. Rotem, F. Vischio, M. Striccoli, E. Fanizza, R. Naaman, D. H. Waldeck, D. Porath and Y. Paltiel, Single Domain 10 nm Ferromagnetism Imprinted on Superparamagnetic Nanoparticles Using Chiral Molecules, *Small*, 2019, **15**, 1804557.
23 N. Goren, T. K. Das, N. Brown, S. Gilead, S. Yochelis, E. Gazit, R. Naaman and Y. Paltiel, Metal Organic Spin Transistor, *Nano Lett.*, 2021, **21**, 8657–8663.
24 H. Al-Bustami, B. P. Bloom, A. Ziv, S. Goldring, S. Yochelis, R. Naaman, D. H. Waldeck and Y. Paltiel, Optical Multilevel Spin Bit Device Using Chiral Quantum Dots, *Nano Lett.*, 2020, **20**, 8675–8681.
25 S. Cardona-Serra, L. E. Rosaleny, S. Gimenez-Santamarina, L. Martinez-Gil and A. Gaita-Arino, Towards Peptide-based Tunable Multistate Memristive Materials, *Phys. Chem. Chem. Phys.*, 2021, **23**, 1802–1810.
26 H. Al-Bustami, G. Koplovitz, D. Primc, S. Yochelis, E. Capua, D. Porath, R. Naaman and Y. Paltiel, Single Nanoparticle Magnetic Spin Memristor, *Small*, 2018, **14**, 1801249.
27 S. M. Reiss, S. Khaldi, O. Shoseyov, S. Yochelis, R. Yerushalmi and Y. Paltiel, Chiral Magnetic Memory Device at the 10 nm Scale Using Self-Assembly Nano Floret Electrodes, *Adv. Electron. Mater.*, 2025, **11**, 2400919.
28 Y. H. Kim, Y. Zhai, H. Lu, X. Pan, C. Xiao, E. A. Gaulding, S. P. Harvey, J. J. Berry, Z. V. Vardeny, J. M. Luther and M. C. Beard, Chiral-Induced Spin Selectivity Enables a Room-Temperature Spin Light-Emitting Diode, *Science*, 2021, **371**, 1129–1133.
29 O. Ben Dor, S. Yochelis, S. P. Mathew, R. Naaman and Y. Paltiel, A Chiral-based Magnetic Memory Device Without a Permanent Magnet, *Nat. Commun.*, 2013, **4**, 2256.

30 Q. Zhu, S. R. Cohen, O. Brontvein, J. Fransson and R. Naaman, Magnetic Monopole-Like Behavior in Superparamagnetic Nanoparticle Coated with Chiral Molecules, *Small*, 2024, **20**, 2406631.
31 S. Ghosh, S. Mishra, E. Avigad, B. P. Bloom, L. T. Baczewski, S. Yochelis, Y. Paltiel, R. Naaman and D. H. Waldeck, Effect of Chiral Molecules on the Electron's Spin Wavefunction at Interfaces, *J. Phys. Chem. Lett.*, 2020, **11**, 1550–1557.
32 M. D. Nguyen, L. Deng, J. M. Lee, K. M. Resendez, M. Fuller, S. Hoijang, F. Robles-Hernandez, C.-W. Chu, D. Litvinov, V. G. Hadjiev, S. Xu, M.-H. Phan and T. R. Lee, Magnetic Tunability *via* Control of Crystallinity and Size in Polycrystalline Iron Oxide Nanoparticles, *Small*, 2024, **20**, 2402940.
33 M. Obaidullaha, N. M. Bahadurb, T. Furusawaa, M. Satoa, H. Sakumaa and N. Suzuki, Microwave Assisted Rapid Synthesis of Fe_2O_3@SiO_2 Core-Shell Nanocomposite for the Persistence of Magnetic Property at High Temperature, *Colloids Surf., A*, 2019, **572**, 138–146.
34 Z.-Y. Tian, Z. Zhang, S. Wang and H. Lu, A Moisture-Tolerant Route to Unprotected α/β-Amino Acid *N*-Carboxyanhydrides and Facile Synthesis of Hyperbranched Polypeptides, *Nat. Commun.*, 2021, **12**, 5810.
35 D. Passeri, C. Dong, M. Reggente, L. Angeloni, M. Barteri, F. A. Scaramuzzo, F. De Angelis, F. Marinelli, F. Antonelli, F. Rinaldi, C. Marianecci, M. Carafa, A. Sorbo, D. Sordi, I. W. Arends and M. Rossi, Magnetic Force Microscopy: Quantitative Issues in Biomaterials, *Biomatter*, 2014, **4**, e29507.
36 S. Schreiber, M. Savla, D. V. Pelekhov, D. F. Iscru, C. Selcu, P. C. Hammel and G. Agarwal, Magnetic Force Microscopy of Superparamagnetic Nanoparticles, *Small*, 2008, **4**, 270–278.
37 E. Skoropata, J. Nichols, J. M. Ok, R. V. Chopdekar, E. S. Choi, A. Rastogi, C. Sohn, X. Gao, S. Yoon, T. Farmer, R. D. Desautels, Y. Choi, D. Haskel, J. W. Freeland, S. Okamoto, M. Brahlek and H. N. Lee, *Sci. Adv.*, 2020, **6**, eaaz3902.
38 T. Sojkova, G. M. R. Rizzo, A. Di Girolamo, S. K. Avugadda, N. Soni, N. B. Milbrandt, Y. H. Tsai, I. Kubena, M. Sojka, N. Silvestri, A. C. Samia, R. Groger and T. Pellegrino, *Chem. Mater.*, 2023, **35**, 6201–6219.